Temperature and Shear Rate Dependence of Small Angle Neutron Scattering from Semidilute Polymer Solutions

I. Morfin,[†,‡] P. Lindner,*[,†] and F. Boué[‡]

Institut Laue-Langevin, BP 156, F-38042 Grenoble Cedex 9, France, and Laboratoire Léon Brillouin, CEN Saclay, F-91191 Gif sur Yvette, France

Received December 4, 1998; Revised Manuscript Received June 15, 1999

ABSTRACT: We use small angle neutron scattering to study the effect of shear on a polymer solution (polystyrene, PS, in dioctyl phthalate, DOP) being in the entangled part of the semidilute regime, in a large range of temperatures and shear rates. The scattering of the induced structure, in the first stages of the flow effect, gives butterfly patterns, i.e., contours constituted of two lobes along the *v* direction. In later stages, as the shear is increased at constant temperature or the temperature is decreased at constant shear rate, the scattering becomes stronger, having greater dependence on *q*, and contours tend finally to have an elliptical shape. This means that the objects created by flow are larger. The temperature effect is not only due to the slowing down of the dynamics of the system at lower *T*, since after correction of the latter, using a time−temperature superposition (determined using oscillatory low strain), the influence of the vicinity of the cloud point on the flow-induced structure remains important. Conversely, steady flow viscosity measured under the same conditions can be corrected using such time−temperature superposition. Some of our results indicate that entanglements are not mandatory to obtain the butterfly effect and that the shear effect can lead to irreversible demixing for solutions closer to the dilute regime.

1. Introduction

Recently, a renewed interest in the flow of complex fluids has arisen, for which the use of optical and in particular scattering techniques have been extended from studies in the quiescent state. In the polymer field, while the study of dilute solutions has taken place for a long time, it appeared rather recently that semidilute solutions (above the concentration c^* of overlapping of the chains) displayed surprising effects as seen by rheooptical and rheoscattering techniques. Rheolight techniques were developed by several groups in the last years, meanwhile only a few experiments involved small angle neutron scattering (SANS). We have extended the latter technique to a more complete study of the most widely studied system (polystyrene in dioctyl phthalate).

The mean goal of this paper is the investigation of the shear rate and temperature dependence of the shear-induced structure in semidilute polymer solutions. A time−temperature superposition of rheological functions (viscosity, normale force) indicates that the influence of the temperature on their macroscopic properties comes from the longest relaxation time of the system only. We show in this present study that it is not the case for the structure visible by neutron scattering, the approach of the demixing temperature at rest enhancing the structuration.

This paper is partitioned in three large parts. After a short recall of the basic characteristics of semidilute polymer solutions in the quiescent state, we review in the first part the principal experiments done using the different techniques mentioned above. In the second part, we present our own experimental results obtained on three different solutions (the first one is in the entangled part of the semidilute regime, the second one is at the limit between the dilute and the semidilute regime, and the third one is in the nonentangled part of the semidilute regime) using rheometry and SANS measurements. The last part of this paper is devoted to a discussion where we consider the temperature dependence of the shear effect and the type of objects created by flow.

2. Background

We will recall below different experiments concerned with solutions having an UCST-type phase diagram as described by Daoud and Jannink.[1] These solutions are in the semidilute regime; the concentration, *c*, is greater than c^*, the overlap concentration ($c^* = M_w/(4\pi N_a R_g^3/3$, where N_a is Avogadro's number and R_g denotes the radius of gyration of one single chain). Depending on the temperature, the quality of the solvent is different: At sufficiently high temperatures compared to the Θ temperature, they are in good solvent (region I in Figure 2); the concentration fluctuations are weak. Around the Θ temperature, the solvent quality is not so good (region II in Figure 2); the concentration fluctuations there are a lot larger than in the good solvent regime. At low temperature (for $T < T_{cl}$, T_{cl} being the demixing temperature), the bad quality of the solvent induces a demixing in solution (region III in Figure 2). The values of T_{cl} as a function of the concentration define the coexistence curve.

We will be concerned with solutions mostly in the Θ solvent regime, for which *c* is slightly or definitely larger than c^*.

2.1. Flow-Induced Turbidity. It has been known for almost 5 decades that flow can induce cloudiness in a large variety of polymer/solvent systems. This behavior occurs above a particular flow rate in many flow geometries, e.g. in a tube (Poiseuille flow), in a cone and plate cell, or in a Couette cell (laminar flow).

In 1974, Verstrate and Philippoff[2] observed visually the appearance of turbidity when semidilute solutions of polystyrene (PS) in dioctyl phthalate (DOP) flow in a capillary tube. In other words, the cloud point (demixing

[†] Institut Laue-Langevin.
[‡] Laboratoire Léon Brillouin.

10.1021/ma981882d CCC: $18.00
Published on Web 09/29/1999

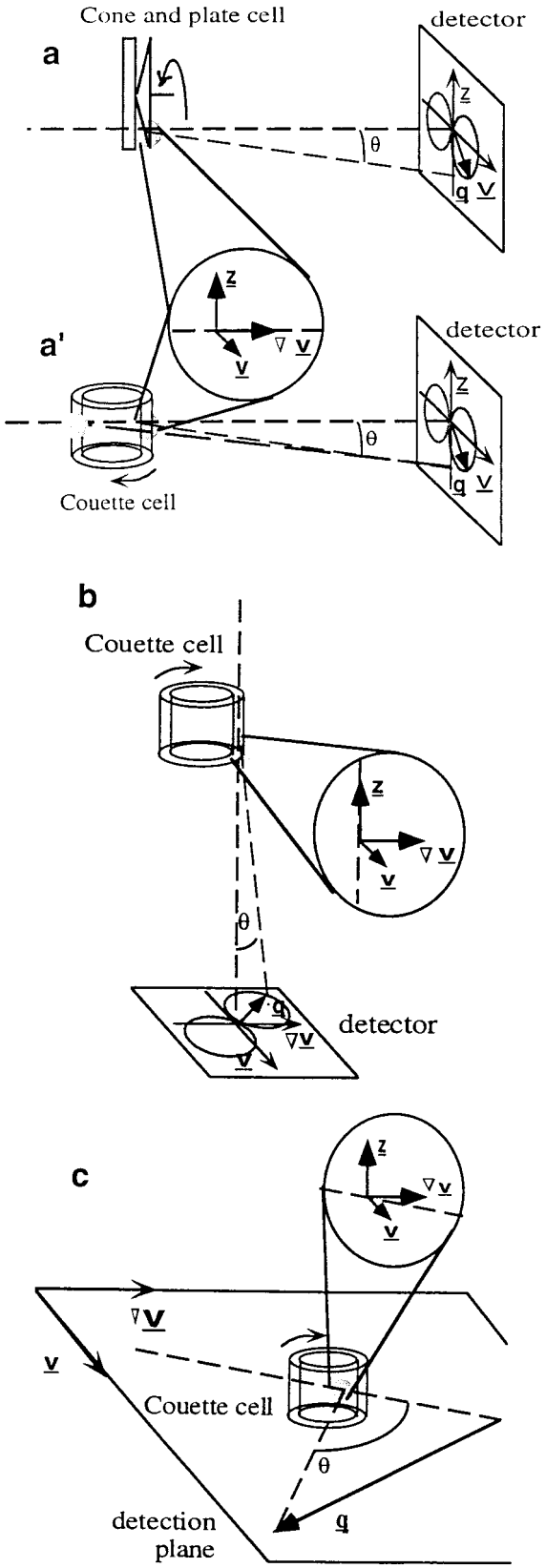

Figure 1. (a, a′) Setups used for SALS[7,14−18] and SANS[24−27] with the (v, z) detection plane. (b) Setups used for SALS[7] with the (v, ∇v) detection plane. (c) Setups used for WALS[6,20,21] with the (v, ∇v) detection plane.

temperature threshold) looks shifted to higher temperature. When increasing the shear flow the cloudiness appears sooner for increasing molecular weight and sooner for decreasing temperature, more precisely when

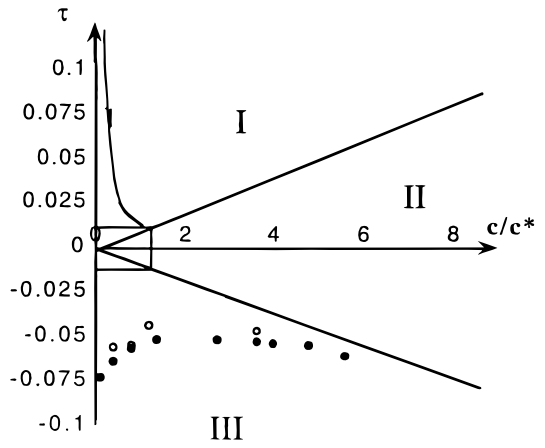

Figure 2. Phase diagram of a nondeuterated (M_w = 520 000) (●) as well as a deuterated (M_w = 572 000) (○) PS in DOP. τ is the reduced temperature; $\tau = (T - T_\Theta)/T_\Theta$.

getting closer to the demixing temperature in the quiescent state.

The influence of concentration seems less obvious but shows a correlation with normal stress. The latter, for a given flow rate, Q, shows a maximum as a function of concentration. At this particular concentration, one observes the largest shift of the cloud point ($T_{cloud}(Q) - T_{cloud}(0)$), ($T_{cloud}(Q)$ being the temperature of demixing for a given flow rate). A review by Rangel-Nafaile et al.[3] of many semidilute or dilute polymer solutions suggests that flow-induced turbidity is a quite general behavior. In some cases, this phenomenon is irreversible.

The theory of Verstrate and Philippoff, discussed in more detail by Rangel-Nafaile, derives the shift of T_{cloud} in a pseudothermodynamic approach. A flow term is added to the Flory−Huggins free energy of mixing between polymer and solvent. This new term corresponds to some elastic energy stored in the chain upon application of the shear which is proportional to the normal stress in the framework of the elastic dumbbell model. This theory gives a good approximation of the demixing temperature for concentrations around the overlap concentration c^* but fails for higher concentrations. In addition, it only takes into account the normal stress, not the shear terms. Finally, this theory, obviously, does not describe the induced structure.

2.2. Shear-Induced Structure. More recently, new models have considered possible flow-induced structures, prompted by new observations using light scattering, microscopy, dichroism, birefringence, and rheology. All these experiments have been done with laminar shear flow. The shear rate is considered as being constant at constant deformation, although NMR experiments have shown some discrepancies.[4]

Helfand and Fredrickson[5] (HF) first proposed a theory that predicts the scattering of a semidilute solution in the plane containing the direction of the flow, v, and the direction of the shear gradient, ∇v, in a low shear regime. Their model is based on the idea that concentration fluctuations, present in solution at rest, are amplified by flow due to the fact that in less concentrated (thus less viscous) regions the displacement of the chains is easier than in more concentrated ones. The authors proposed that, due to flow, the chains could migrate toward the concentrated zones and increase the spatial fluctuations of concentration. Since a maximum in the scattering function was observed experimentally,[6,7] modified models took into account the time (τ_r)

necessary for the polymer to respond to flow.[8] It has been argued that the characteristic time for concentration fluctuations to develop over a size $1/q$, $\tau_{dev} = 1/(D_{coop}q^2)$, has to be larger than this time τ_r. This defines a maximum for $q = 1/(D_{coop}\tau_r)^{1/2}$. This idea has been first proposed by Brochard and de Gennes in order to describe fast and slow modes in polymer solutions.[9] Other models were proposed by Doi et Onuki,[10] Helfand,[11] and Van Egmond.[12] A review of these different theoretical approaches can be found in ref 13.

On the experimental side, many scattering studies[6,7,14−21,24−27] have involved the PS/DOP system because of its experimental advantages coming from the relatively high viscosity and the nonvolatility of DOP and the Θ temperature of the solution, which is around room temperature. Experiments were done with a large variety of molecular weights, concentrations, and temperatures. Unfortunately, we will see that the various experimental conditions make it difficult to compare the different studies and to establish some general trends. One important consequence of this variety is that the shear rates reported by the different groups cannot be classified in a common scheme. For instance, low (or high) shear rate conditions as discussed below do not correspond to the same shear rate for different experiments.

Moreover, the different experiments involved different ranges of momentum transfers, different setups as well as different detection planes. They are represented in parts a, a′, b, and c of Figure 1. Because of the complexity due to the great variety of experimental conditions, we feel the need to review briefly the different experiments before presenting our results. We have to distinguish between different kinds of techniques which explore a large range of lengths, from the macroscopic scale where the turbidity can be seen by eye down to the scale of the polymer segment length.

2.2.1. Large Scales: Small Angle Light Scattering (SALS), Microscopy. Small angle light scattering, used by Fuller et al.[7,14] and Hashimoto et al.,[14−18] investigates the very low q range ($6.3 \times 10^{-5} < q$ [Å^{-1}] $< 3 \times 10^{-4}$). Both groups used solutions in the entangled part of the semidilute regime. We would like to point out that these experiments were done with large molecular weight polystyrene ($M_w > 10^6$) around ambient temperature. The solutions were sheared in different types of shear devices.

For a cone and plate cell (Hashimoto et al.)[14−18] or a plate and plate cell (Fuller et al.),[7] the laser beam goes through the sample parallel to the shear gradient. The scattering is detected in the (v, z) plane perpendicular to it (v, being the direction of the velocity, z being the neutral direction or vorticity direction) (Figure 1a).

For a Couette cell (Fuller et al.),[7] the laser travels between the two cylinders, parallel to their axis. In this case, the detector plane is the (v, ∇v) plane (Figure 1b).

The SALS experiments of Hashimoto et al. have been directly coupled with rheology measurements and microscopy.[18] Three different regimes of shear rates have been defined in the Θ temperature region.

(1) Below a threshold, noted as $\dot{\gamma}_c$, the viscosity, η, and the first normal stress coefficient, ψ_1 ($\psi_1 = N_1/\dot{\gamma}^2$, with N_1, the first normal force difference, equal to $\sigma_{11} - \sigma_{22}$, σ_{ii} being the normal stresses), are constant when plotted as a function of the shear rate. In terms of Weissenberg numbers, $\dot{\gamma} < \dot{\gamma}_c$ corresponds to $Wi < 1$. Wi is a nondimensional parameter taking into account the variation of the longest relaxation time of the solution with temperature ($Wi = (\tau_r\dot{\gamma})$, and τ_r is usually defined as the point where η/η_o becomes significantly lower than 1). In this regime, the light scattering does not display any change: the two-dimensional pattern is isotropic and identical to the one observed in the quiescent state. Thus, no changes in the structure are revealed in this regime, at least in the plane (v, z).

(2) Above $\dot{\gamma}_c$ (corresponding to $Wi = 1$), flow induces changes of rheological properties: shear thinning is visible on both the viscosity, η, and the first normal stress coefficient, ψ_1. The scattered intensity increases in the v direction without any change in the z direction; this is first visible on the total integrated intensities along one direction, and at larger $\dot{\gamma}$, also on 2D spectra. The effect is seen as a "dark streak" in the z direction. At about 10 times larger shear rates, the contours of the scattered intensity display clearly a butterfly shape with lobes along the v direction (symmetric with respect to the z direction). This scattering has been interpreted in terms of enhancement of concentration fluctuations leading to regions more or less concentrated in polymer which are oriented in some preferential directions around the neutral direction z. A maximum of the intensity at finite q indicates a periodicity of a few microns of the induced structure. Such structure can be visualized by microscopy. This suggests that the contrast between regions rich and poor in polymer is large, as in a system undergoing a phase separation.

For high shear rates $\dot{\gamma} > \dot{\gamma}_a$ (corresponding to large Wi in the investigated temperature range), rheological anomalies such as a sudden increase of η and ψ_1 are observed, meanwhile the overall intensity increases strongly and a long streaklike pattern appears in the z direction. This is interpreted as long stringlike objects (droplets) aligned parallel to the flow. This structure has also been visualized by microscopy. It seems that the droplets rich in polymer can be extremely elongated without breaking (this seems to be observed also in conditions of deep quench in the two-phase region[19]). It also looks as if high concentrated regions which first grew around the z direction at lower shear rate have now tilted by 90°. However, butterfly patterns can be present simultaneously with the light streak.[17]

Fuller et al.[7] investigated scattering after onset and cessation of the flow in about the same range of q but in the (v, ∇v) plane. They observed anisotropic patterns constituted of two lobes symmetric with respect to the incident beam axis ($q = 0$). As they start or stop the flow, they observe that the axis joining the center of the lobes rotates.

2.2.2. Wide Angle Light Scattering (WALS). Wide angle light scattering has been used by Pine et al.[6,20,21] to investigate momentum transfers contained also in the (v, ∇v) plane (i.e. as did Fuller[7] et al. with SALS at low q and at variance with Hashimoto et al.[14−18]). Equal intensity contours are built from successive measurements done at different angles between the detector and the light beam, for different positions of the beam with respect to the velocity vector (Figure 1c). Momentum transfers q are higher than for SALS ($5 \times 10^{-4} < q$ [Å^{-1}] $< 3 \times 10^{-3}$); hence WALS gives structural information at lower length scale than the experiments of Fuller et al.[7]

Dixon et al.[6] first studied a polystyrene (PS) of $M_w = 1.86 \times 10^6$ in DOP for $Wi \approx 1$. In contrast to the observations made at low q by SALS (see above), the

scattered intensity becomes anisotropic for the smallest shear rates. The contours have mostly the same shape as observed at lower q in this plane: they consist of two lobes symmetric with respect to the origin ($q = 0$). Inside each lobe, one observes a maximum at finite q.

For Weissenberg numbers smaller than unity ($Wi < 1$), this maximum appears at an angle $\beta = 45°$ (β being the angle between the velocity and the q direction). The peak rotates toward $\beta = 0°$ as Wi increases toward 1, then becomes negative, and finally approaches $\beta = -45°$ for higher Wi. This behavior is partially in agreement with the model based on the enhancement of concentration fluctuations.[5,8]

The same group, using the same technique,[20] performed transient light scattering measurements upon cessation of the shear with the same sample and showed that the mechanism of enhancement of concentration fluctuations selects only the slow mode of diffusion (semidilute polymer solutions have two modes of diffusion, the gel mode and the slow mode, as shown by several authors[9]). This sheds more light on the origin of the peak observed in the steady state as described just above and which is discussed in the model of Milner.[8]

Finally, Pine's group investigated the high shear rate regime.[21] An increase of the intensity in all directions for $Wi \gg 1$ appears superimposed on the low shear signal with maxima along the y direction. Time dependencies of transient scattering measurements after cessation or initiation of the shear allowed them to separate the signal in two contributions: (1) a signal having a peak at $\beta = -45°$, similar to the signal obtained at "moderate" Wi, which would be the response of the concentration fluctuations, and (2) a signal responsible for the maxima along the y direction. This last one is very strong, and has a time evolution which is on a longer scale than the first one. It is interpreted by the authors as the result of a demixing process.

2.2.3. Dichroism and Birefringence. Dichroism and birefringence measurements confirm results obtained by SALS as well as by WALS and give additional information.[7,22,23]

Scattering dichroism is sensitive to the orientation of large objects. For weak shear rates, dichroism measurements in the (v, z) plane[7] show that concentration fluctuations create predominantly concentrated domains aligned parallel to the neutral direction (corresponding to scattering along the flow direction). For higher shear rates, the objects are oriented parallel to the flow. Dichroism measurements in the (v, ∇v) plane[7] indicate that the concentrated domains orient and grow along an axis at $\beta = -45°$ to the direction of flow (corresponding to large scattering in the direction 45° in the reciprocal space) in the range of low or moderate shear rates.

Birefringence is sensitive to the local orientation of the chain, which dominates the form effect here. Measurements indicate that segmental orientations occur along the flow direction at low shear rate. For higher flow, corresponding to dichroism changes as well as shear thickening, birefringence indicates a strong local orientation along the flow direction. But the most striking feature is its variation with time, which, surprisingly, becomes erratic.

2.2.4. Small Angle Neutron Scattering (SANS). Small angle neutron scattering is the third scattering technique used, until now, only in the (v, z) plane (Figure 1a′). This is the same plane as for the SALS experiments of Hashimoto et al., but there is no overlap with the momentum transfers q, accessible by SALS.

SANS gives structural information at a lower length scale than light scattering. Hammouda et al.[24] and Nakatani et al.[25] respectively explored the following range of q: $3 \times 10^{-3} < q$ [Å^{-1}] $< 1.3 \times 10^{-2}$ and $8 \times 10^{-3} < q$ [Å^{-1}] $< 6.2 \times 10^{-2}$. Previous experiments of Boué and Lindner[26,27] covered a range of q between 2×10^{-3} and 2×10^{-1} Å^{-1}. As we will see below, we extend SANS studies to smaller q in the present paper.

Boué and Lindner[26,27] investigated the low as well as the high shear rate regime, using a polymer of lower molecular weight than all the experiments mentioned above. At low shear rates (for example $T = 22$ °C and $\dot{\gamma} = 6.8$ s^{-1}), they observed an anisotropy of the SANS pattern, with an increase of the scattering in direction parallel to the flow. As for the SALS experiments described above (section 2.2.1), the shape of the pattern resembles a butterfly which has its wings in the v direction. The intensity parallel to the flow direction increases for $q < 1/\xi_1$ compared to the intensity at rest as the shear rate increases. ξ_1 is the correlation length at rest obtained by fitting the scattering cross section $d\Sigma/d\Omega$ as a function of q with an Ornstein Zernike law:

$$d\Sigma/d\Omega(q) = d\Sigma/d\Omega(0)/(1 + q^2\xi_1^2) \qquad (1)$$

For $q > 1/\xi_1$, the intensity in the v direction is lower than the scattering at rest. The shape of the pattern at large q values then resembles an ellipse. This signals that the chain appears stretched when observed along the v axis. No change of the intensity in the perpendicular direction is observed in either q range.

In a high shear rate regime, Boué and Lindner[27] observed that the onset of turbidity in solution is accompanied by a strong increase of the SANS intensity in *all directions* at low q. This seems to mask the butterfly shape in such a way that anisotropy is no longer detectable in the contours. Such an isotropic pattern is mostly in agreement with the results of Hammouda et al.[24] and Nakatani et al.,[25] who studied the scattering of PS/DOP solutions in the shear range where solutions are indeed turbid. They observed a strong increase of the intensity in all directions at low q, the isointensity curves being isotropic or slightly anisotropic.

2.2.5. Summary. This ensemble of experiments indicates two regimes of flow-induced structure. First, an anisotropic structure is created by flow even at low shear ($Wi \geq 1$), at least at the relatively low length scale accessible by SANS and WALS. The projection of the objects on to the (v, z) plane orients preferentially around the z direction and the projection of the objects on to the (v, ∇v) plane orients along a direction $\beta = +45°$ with respect to the flow direction for low shear rates. Second, the situation is modified for larger shear rates. On one hand, the effects extend to a larger length scale, becoming visible by SALS, by microscopy, and finally by eye. Thus, the cloudiness can be due to an anisotropic scattering which itself is due to the flow-induced anisotropic structure. On the other hand, it is not clear whether the large shear structure is a consequence of the low shear structure or of shear-induced demixing (producing larger objects which in turn can have their own anisotropic spatial correlations).

Table 1. Review of the Different Molecular Weights, Concentrations, Reduced Concentrations, and Temperatures Investigated by Us and by Other Groups

M_w (g/mol)	concn (% w/w)	c/c^*	temp (°C)	ref	authors
5.72×10^5	9	3.6	$1.7 < T < 50$	present work	
5.72×10^5	3.45	1.4	11	present work	
3.50×10^4	14	2.4	4	present work	
5.72×10^5	9	3.6	$15 < T < 30$	26, 27	Boué et al.
5.48×10^6	3, 6	20, 40	$21 < T < 27$	14−18	Hashimoto et al.
3.84×10^6	6	30	21, 22	14	Kume et al.
1.8×10^6	4	5	15	6	Wu et al.
1.86×10^6	4	5	15.3	20	Dixon et al.
1.07×10^6	4	2.5	15	21	Migler et al.
1.86×10^6	6	6	$12 < T < 20$	7, 14	Fuller et al.
1.0×10^6	6	3	$15 < T < 40$	23	Moldenaers et al.
1.8×10^6	6	6	$15 < T < 40$	23	Moldenaers et al.
4×10^6	6	35	$15 < T < 40$	25	Nakatani et al.
1.81×10^6	3	2	22	24	Hammouda et al.

The different experiments are difficult to correlate because of the differences in molecular weight, shear rate, temperature, and concentration. It seems, however, that—in addition to the stretching of chains—flow creates an anisotropic structure on a low length scale before structuration on a larger length scale appears. Moreover, flow effects are still visible by SANS for high shear rates (in the turbid regime). Neutron scattering in conjunction with laminar flow thus gives us the possibility to investigate a rather wide range of experimental conditions (shear rates and temperatures) on length scales where not a lot of information is available in the literature. The experiments reported here keep the same system as studied earlier.[26,27] Additional measurements on solutions with a different concentration or a different molecular weight will also be shown.

3. Experimental Section

3.1. Polymer and Solvent. Most of the rheology and SANS measurements of this paper were performed with the same system as the one previously investigated by Lindner and Boué (called "solution 1" below). The polymer is deuterated linear polystyrene (d-PS synthesized by anionic polymerization). The molecular weight obtained by size exclusion chromatography is around $M_w = 572\,000$ g/mol (degree of polymerization = 5107), and the polydispersity (M_w/M_n) is 1.12. The solvent is nondeuterated dioctyl phthalate (bis(2-ethylhexyl)-phthalate, "DOP", from Aldrich). Due to the replacement of protons by deuterium in the PS chains, the Θ temperature is not $T_\Theta = 22$ °C, as determined for the PS/DOP solution.[28] We determined T_Θ to be around 7 °C by measuring the second virial coefficient of a concentration series in the dilute regime as a function of the temperature ($T = T_\Theta$ when $A_2 = 0$) by WALS as well as by SANS. Solution 1 has a polymer concentration $c = 9\%$ ($c^* = 2.5\%$). The demixing temperature of our d-PS/DOP solution 1, i.e., the cloud point, measured by turbidity is $T_{cloud} = -6 \pm 1$ °C for this concentration.

Our experiments cover a large range of temperatures between 2 and 50 °C, which includes the whole Θ regime.

We also used a solution of the same polymer at a lower concentration $c = 3.45\%$ (called "solution 2" below), closer to the concentration c^*, in order to study the influence of chain overlapping. We show (Figure 2) the phase diagram of the deuterated ($M_w = 572\,000$) as well as a protonated ($M_w = 520\,000$) PS in DOP.

Finally, we used "solution 3", for which the molecular weight is $M_w = 35\,000$, the polydispersity $M_w/M_n = 1.05$, and the concentration $c = 14\%$, in order to investigate the purely nonentangled regime.

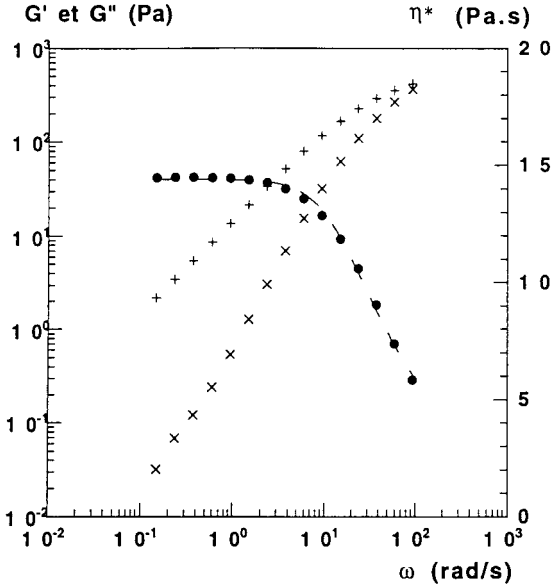

Figure 3. Storage modulus G' (×), loss modulus G'' (+), and complex viscosity $|\eta^*(\omega)|$ (●), as a function of ω, at $T = 22$ °C. The dashed line is a Carreau fit of $|\eta^*(\omega)|$.

For comparison, we summarize in Table 1 the different molecular weights, concentrations, and temperature ranges used in our experiments as well as for those of other groups.

3.2. Rheology. Rheology measurements were performed on solution 1 in order to associate the macroscopic properties of the solution under shear with the structural changes observed by SANS. The rheometer is a Rheometrics RFS II, in cone and plate geometry.

We first measured the complex viscosity $|\eta^*(\omega)|$ ($\eta^*(\omega) = (G'' - iG')/\omega$, G'' and G' being, respectively, the loss modulus and the storage modulus) as a function of the frequency ω (in rad/s) at several temperatures T (Figure 3 shows G', G'', and $|\eta^*(\omega)|$ versus ω for $T = 22$ °C). In these oscillatory measurements, the strain amplitude is between 5% and 30%, depending on the temperature, but is chosen to be low enough to remain in the regime of low deformation. The fit of $|\eta^*(\omega)|$ with a Carreau law

$$|\eta^*(\omega)| = |\eta^*_0|(1 + (\omega\tau_r)^2)^{-n/2} \qquad (2)$$

gives access to the longest relaxation time of the system, τ_r, for each temperature. The variations of $|\eta^*_0|$ and τ_r

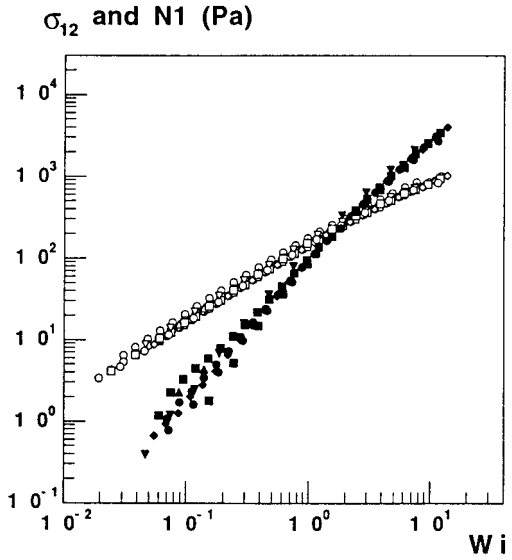

Figure 4. Shear constraints σ (empty symbols) and first normal forces difference N_1 (filled symbols) as a function of *Wi* for a series of temperatures between 2 and 30 °C.

as a function of temperature follow an Arrhenius law with about the same activation energy:

$$|\eta^*(0)| = 2.98 \times 10^{-10} \exp(7258/T) \quad (3)$$

$$\tau_r = 1.28 \times 10^{-12} \exp(7311/T) \quad (4)$$

Knowing τ_r for all temperatures investigated in our SANS experiments, we can calculate the Weissenberg number ($Wi = \dot{\gamma}\tau_r$) for the different ($\dot{\gamma}$, T) conditions.

We then performed a second series of experiments, applying steady shear to the solution in a large range of shear rates and temperatures, under conditions similar to our SANS measurements, apart from the fact that the SANS experiments were done in a Couette cell. Figure 4 represents the shear stress, σ_{12}, as well as the first normal stress difference, N_1, for several temperatures between 2 and 30 °C. For both σ_{12} and N_1, the plots as a function of *Wi* (calculated according to eq 4) are superimposed for the different temperatures. They define two master curves revealing the relevance of the nondimensional parameter *Wi* in rheology.

The shear viscosities, η and η^*, as a function of *Wi*, have a similar profile for each investigated temperature:[29] for $Wi < 1$, the viscosities are constant, and for $Wi > 1$, the viscosities decrease as the shear rate increases (non-Newtonian shear thinning). They, however, do not precisely follow the empirical Cow−Merz law since the decreasing part is more pronounced for η^* than for η (Figure 5).

The normal stress difference becomes nonnegligible for $Wi \approx 0.1$ and even dominant for $Wi > 1$. This well displays the non-Newtonian response of this solution under shear, due to the storage of elastic deformation.

We did not detect any shear thickening (increase of $\eta(\dot{\gamma})$) at high *Wi*, at variance with refs 16 and 22. That is to say, our measurements do not extend into the regime of shear rates $\dot{\gamma} > \dot{\gamma}_a$, as defined by Hashimoto et al.[16] It seems, however, in Figure 5 that the shear thinning for $\eta(Wi)$ slows down for the highest *Wi* investigated. This is a slight indication that shear thickening could appear for *Wi* larger than 50 with our solution 1.

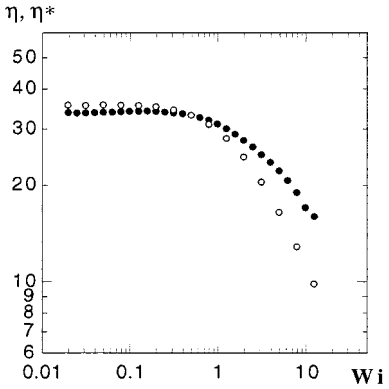

Figure 5. $\eta(\omega)$ and $\eta(\dot{\gamma})$ as a function of the *Wi* at a same temperature (T = 11 °C).

In summary, both for oscillatory and for steady shear measurements, *Wi* is the appropriate parameter for a time−temperature superposition. Later in the paper, we will check whether SANS measurements for different T and $\dot{\gamma}$ depend or not upon *Wi* as it does for the mechanical functions.

3.3. SANS Experiments. Small angle neutron scattering experiments were performed on instrument D11 of the Institut Laue-Langevin ILL, Grenoble, France. The solution is sheared in a Couette cell made of quartz glass.[30] The inner cylinder (stator) has an outer diameter of 47 mm and the outer cylinder (rotor) has an inner diameter of 48 mm, giving a total effective sample thickness of 1 mm. The regulation of the temperature is done by circulation of water in compartments positioned inside the inner cylinder, on either side of the beam path. The temperature is measured by a platinum resistor (Pt 100). The condensation of humidity is avoided by circulation of dry air around the Couette cell. The neutron beam passes through the sample in the direction parallel to the shear gradient and perpendicular to the flow direction (Figure 1a′). The scattering is recorded in the (v, z) plane (with z being the neutral direction), on a position sensitive multidetector at three distances away from the sample (D = 2.5, 10, and 35.7 m, the collimation distances being respectively 5.5, 10.5, and 40.5 m). With wavelengths of λ = 10 and 14 Å, the effective range of momentum transfer ($q = 4\pi/\sin(\theta/2)$, θ being the scattering angle) is $8 \times 10^{-4} < q$ [Å^{-1}] $< 8 \times 10^{-2}$. The neutron scattering intensity is normalized with the scattering of a 1 mm thick water sample as standard reference, measured in the Couette cell at a distance D = 2.5 m. All spectra are corrected for the detector background and empty cell scattering. After subtraction of the corrected solvent spectrum, we obtain differential cross sections in v and z directions, $d\Sigma_v/d\Omega(q,\dot{\gamma})$ and $d\Sigma_z/d\Omega(q,\dot{\gamma})$, by radial integration respectively over an angular sector of 30° around the v direction and over an angular sector of 15° around the z direction. We then plot them as a function of the momentum transfer q. Two-dimensional contour patterns are also shown in this paper. Their lines represent isointensity curves (a curve closer to the beam stop corresponds always to a higher intensity for these experiments). The indicated values correspond to the logarithm of the differential scattering cross section $d\Sigma/d\Omega$ (in the following also denoted as "intensity").

4. Results from SANS

We have chosen to describe the data starting from a series done at constant temperature and show the

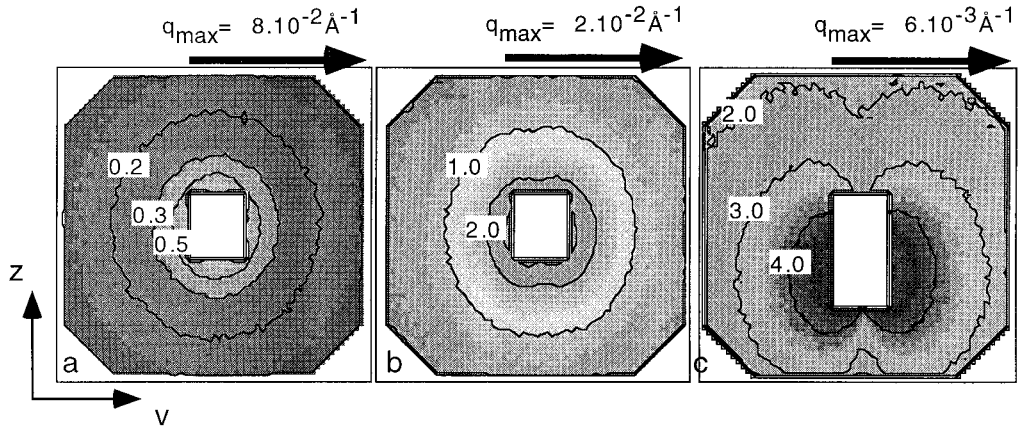

Figure 6. Contour plots of two-dimensional scattering patterns obtained at D11 ($\lambda = 10$ Å) with the sample detector distances $D = 2.5$ m (a), 10 m (b), and 35.7 m (c), at a shear rate $\dot{\gamma} = 300$ s^{-1} and temperature $T = 22$ °C. The indicated values are log(dΣ/dΩ). The beam stop (rectangular shape at the center of the patterns) is bigger at 35.7 m; this is due to the normalization by water scattering measured at 2.5 m.

dependence upon shear. We will then try to connect the results to the dependence upon temperature in order to test a time−temperature superposition. Finally, we will report a few results for the other solutions, 2 (more dilute) and 3 (not entangled).

4.1. Influence of Shear. Let us first consider a series of measurements made at constant temperature $T = 22$ °C. This temperature corresponds to the Θ-point of the nondeuterated PS/DOP, which is about 15 °C above the d-PS/DOP Θ-point. The shear rates used ($12.5 < \dot{\gamma}$ [s^{-1}] < 300, i.e., $0.9 < Wi < 23$) are in the range where shear thinning is observed by rheology (Figure 5); solution 1 is never turbid during these experiments. The two-dimensional SANS patterns are anisotropic for all q. Results are presented for the three detector distances in Figure 6a−c.

We split the description into two q ranges.

4.1.1. At High *q*. We define this range by $q > 1/\xi_1$ ($\xi_1 = 53$ Å at $T = 22$ °C). In this range, only a slight change of the scattering under shear compared to the scattering at rest is visible. It leads to elliptical isointensity curves with the major axis of the ellipses along the z direction (Figure 6a).

Correspondingly, the intensity in the v direction, dΣ_v/d$\Omega(q,\dot{\gamma})$, is lower than the intensity at rest, dΣ/d$\Omega(q,\dot{\gamma} = 0)$, for all shear rates, indicating an elongation of the chains in this direction.

The intensity in the z direction dΣ_z/d$\Omega(q,\dot{\gamma})$ remains the same as dΣ/d$\Omega(q, \dot{\gamma} = 0)$: the neutral direction indeed corresponds to no deformation, as reported before.[26]

4.1.2. At Low *q*. For $q < 1/\xi_1$, the changes with respect to the scattering at rest are more pronounced, as can be seen in Figure 6c ($\dot{\gamma} = 300$ s^{-1}, $Wi = 22.3$). In contrast to the high q range, the intensity under shear is stronger than the one at rest for all q directions, except the case of very low shear rates, where the intensity in the z direction does not sensibly vary compared to the scattering at rest.[26] The effect of shear can be seen by comparing Figure 6c (300 s^{-1}) with Figure 7 ($\dot{\gamma} = 125$ s^{-1}, $Wi = 9.3$), which cover the same range of q. In both spectra, the isointensity curves resemble a butterfly with two elliptical lobes having their major axis parallel to the neutral direction z and their centers on the v axis. As the shear rate is increased (comparing Figure 7 with Figure 6c), the q range where

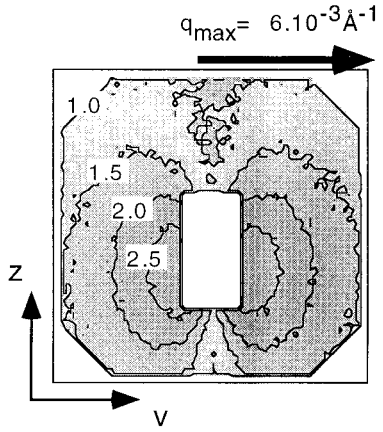

Figure 7. Contour plots of the two-dimensional scattering patterns obtained at $D = 35.7$ m ($\lambda = 10$ Å), at a shear rate $\dot{\gamma} = 125$ s^{-1} and at a temperature $T = 22$ °C. The indicated values are log(dΣ/dΩ).

the butterfly anisotropy is present seems to be shifted toward smaller q.

In the two preferential directions previously defined, this feature corresponds to (i) an increase of dΣ_v/d$\Omega(q,\dot{\gamma})$ with the shear rate along the flow direction. Toward lower q, the intensity shows a steep upturn and then a plateau in the very low q range in the direction parallel to the flow (Figure 8a). This is confirmed by an experiment done at $\lambda = 14$ Å, also shown in Figure 8a. We can decompose dΣ_v/d$\Omega(q,\dot{\gamma})$ as a sum of a Lorentzian at large q, with a correlation length ξ_2 slightly larger than ξ_1 (measured at rest), plus either a Lorentzian (cf. eq 1) with a new correlation length, Ξ_{Lor}, or a Debye−Bueche function (squared Lorentzian),

$$d\Sigma/d\Omega(q,\dot{\gamma}) = d\Sigma/d\Omega(0,\dot{\gamma})/(1 + q^2\Xi_{Deb}^2)^2 \qquad (5)$$

with a new correlation length $\Xi_{Deb} = \Xi_{Lor}/2$ at low q. A better fit is indeed obtained with the Debye−Bueche function for the high q range. We therefore give in Table 2 the results for Ξ_{Deb} and dΣ_v/d$\Omega(0, \dot{\gamma})$ following from eq 5.

The butterfly anisotropy also corresponds to (ii) an increase of dΣ_z/d$\Omega(q,\dot{\gamma})$ with shear rate. Let us note that dΣ_v/d$\Omega(q,\dot{\gamma}) >$ dΣ_z/d$\Omega(q,\dot{\gamma})$ in this q range for all applied shear rates. The low q upturn does not show any plateau in this low q part (Figure 8b): the variation of dΣ_z/dΩ-

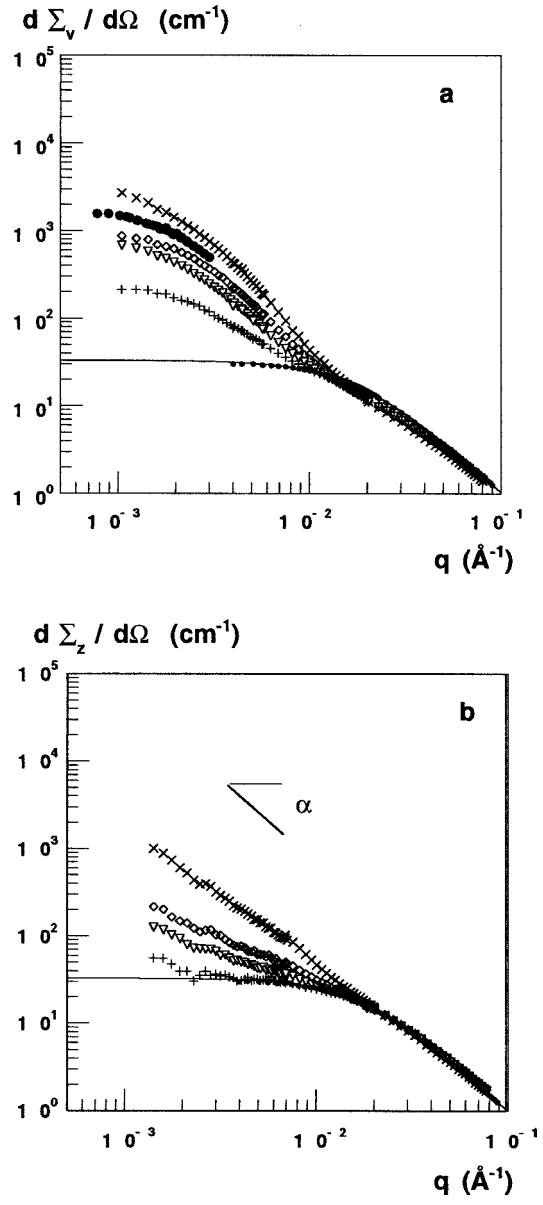

Figure 8. Coherent differential scattering cross section $d\Sigma/d\Omega$ (cm^{-1}) as a function of the momentum transfer q at $T = 22$ °C and several shear rates: $\dot\gamma = 75\ s^{-1}$ (+), $\dot\gamma = 150\ s^{-1}$ (▽), $\dot\gamma = 225\ s^{-1}$ (◇), $\dot\gamma = 250\ s^{-1}$ (●) and $\dot\gamma = 300\ s^{-1}$ (×), in the v direction (a) and in the z direction (b). ● corresponds to an experiment done with $\lambda = 14$ Å (only $d\Sigma_v/d\Omega$ is shown for this particular configuration). The full line is the Ornstein−Zernike fit of $d\Sigma(\dot\gamma = 0)/d\Omega$ for $T = 22$ °C.

Table 2. $d\Sigma_v/d\Omega$ (cm^{-1}) at $q = 0$ and Correlation Lengths Ξ_{Deb} Obtained by Fitting Curves of Figure 6a with the Debye−Bueche Function

shear rate (s^{-1})	$d\Sigma/d\Omega(0)$ (cm^{-1})	Ξ_{Deb} (Å)
12.5	13	117
75	221	250
150	454	269
225	973	276
300	3206	353

$(q,\dot\gamma)$ follows an apparent power law $q^{-\alpha}$. We do not consider this power as the sign of a fractal structure since it is only observed over one decade of q. However, for the sake of simplicity, we will use α to quantify the variation at low q in the forthcoming discussion. For this series of experiments at $T = 22$ °C, α increases linearly with Wi from 0.1 to 1.5. This can be due to an increase of the sharpness of the surface between different zones.

We interpret the signal in the z direction, which is the neutral direction as far as macroscopic flow is concerned, as a sign of the nonlinearity of the response of the system. In some cases, flow instabilities may have the same consequences, but the increase of the intensity in the z direction appears at relatively low shear rates, far below the shear rates where we observe Weissenberg instability in the Couette cell and far below the shear rates inducing anisotropy by SALS. This feature could be a sign of the demixing in the solution or related to the normal forces present in such systems as previously mentioned. Let us recall that observations with the same solution at lower shear rates ($\dot\gamma = 6.8\ s^{-1}$, at $T \approx 22$ °C)[26] show an initial regime with no changes in the $d\Sigma_z/d\Omega(q,\dot\gamma)$.

4.1.3. Experimental Limitations for High Shear. Experiments at shear rates higher than 300 s^{-1} for $T = 22$ °C could not be performed because of the onset of Weissenberg instabilities: we recall that the Couette cell is open at the top and has a free meniscus, i.e., the liquid−air interface is mechanically not confined. Above some critical shear rate, the fluid will rise up the gap due to normal forces. Voids in the form of bubbles, which become strongly elongated along the flow direction, are progressively created and the solution will finally overflow out of the container. The scattering volume is thus becoming inhomogeneous and makes a quantitative data treatment impossible.

4.2. Influence of the Temperature. In a second set of experiments, we observed the same sample in a large range of temperatures, between 2 and 50 °C. Let us first consider a series of experiments made at constant shear rate $\dot\gamma = 165\ s^{-1}$ in a narrow temperature range, 14.7 °C < T < 25.4 °C, i.e., relatively close to $T = 22$ °C. We will see that the trends observed at these temperatures can be extended to a larger range of T and $\dot\gamma$, as shown in the next section.

For $\dot\gamma = 165\ s^{-1}$, the butterfly shape at a detector distance $D = 35.7$ m is visible for all T between 14.7 and 25.4 °C; this corresponds to Wi between 9 and 23. However, we observed that the lobes move toward lower q values as the temperature decreases (Figure 9). This behavior is *qualitatively the same* as the one obtained at constant temperature and increasing shear rates (Figures 6a and 7). It can also be seen by comparing the plots representing $d\Sigma_v/d\Omega(q,\dot\gamma)$ and $d\Sigma_z/d\Omega(q,\dot\gamma)$ versus q for the two sets of experiments, i.e., Figures 8a,b (constant T, variable $\dot\gamma$) and 10a,b (constant $\dot\gamma$, variable T).

However, for a given Wi, the scattering still depends on T. This is seen in figures 9a and 6c, both corresponding to $Wi \approx 23$: the butterfly shape shows up only at very low q for $T = 14.7$ °C, while it is present at all q for $T = 22$ °C. We reach here an important point of this paper: the parameter Wi is not sufficient to relate the variation of scattering with shear rate; in contrast to rheology, there is no time−temperature superposition as far as scattering is concerned. At lower temperature, the change from butterfly to elliptical shape occurs sooner, i.e., at a lower Wi.

4.3. Generalization for a Large Range of Temperatures and Shear Rates. We have extended our SANS measurements to a series of lower temperatures (2 < T [°C] < 11). We observe that there is always a range of shear rates where the two-dimensional SANS

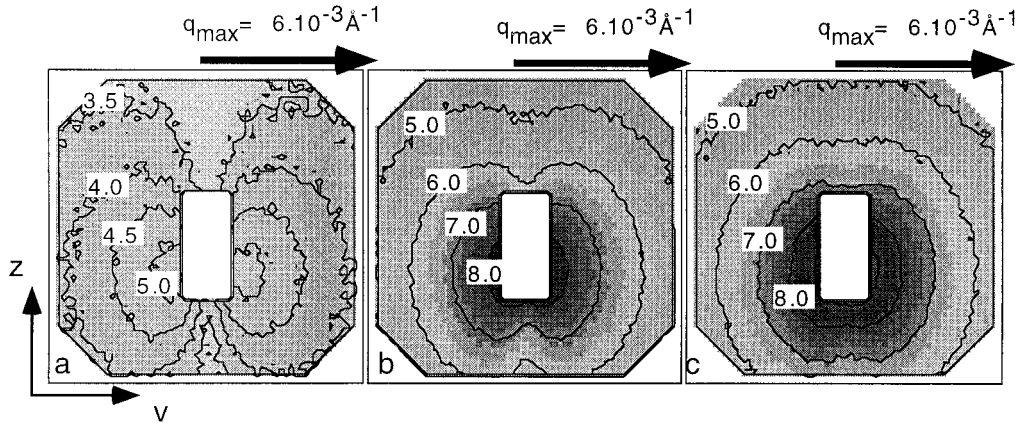

Figure 9. Contour plots of two-dimensional scattering patterns obtained at $D = 35.7$ m ($\lambda = 10$ Å), at shear rate $\dot{\gamma} = 165$ s^{-1} and several temperatures $T = 25.4$ °C (a), $T = 16.5$ °C (b), and $T = 14.7$ °C (c). The indicated values are log(dΣ/dΩ).

patterns change from a butterfly to an elliptical shape. Figure 11, showing patterns obtained at three different shear rates and at $T = 3.5$ °C, is a good illustration of this feature. Let us note the particularly low values of shear rates involved in this measurement.

For the low-temperature measurements (Figure 12), no flow-induced correlation lengths, Ξ_{Deb}, can be extracted in the *v* direction (see in contrast section 4.1.2); i.e., there is no plateau at low *q*. This indicates again that the scattering is shifted toward lower *q* as the temperature decreases. We could, however, study the evolution of the scattering as a function of *Wi* in the perpendicular direction by looking at the variation of the exponent α defined above. We report in Figure 13 the values of α as a function of *Wi* for all temperatures investigated. We can note that α increases linearly with *Wi* for a given temperature, but faster and faster with respect to *Wi* as the temperature decreases (as seen from the results at $T = 22$, 11, and 3.5 °C). No value higher than 3.4 was obtained, because the onset of flow instabilities and the creation of bubbles made an extension of the study impossible at larger *Wi* for each temperature investigated.

Let us note that the anisotropy already appears at $Wi < 1$ for the lowest temperatures. In the literature, changes happening at $Wi < 1$ have been reported in WALS experiments but not in SALS.

Finally, no irreversibility was observed after cessation of the flow in the whole range of investigated temperatures, at least in the time range of our experiments (few minutes).

4.4. Influence of the Entanglements and the Approach of the Dilute Regime. We present here some results for two other polymer solutions.

4.4.1. Solution with No Entanglements. One possible origin of the anisotropic scattering is entanglements. They are an ingredient of the theory for the maximum observed in the light scattering regime.[6] Depending on how many blobs are necessary to form an entanglement, our solution 1 can be considered as more or less entangled. Anyhow, it is interesting to study a solution of d-PS of small molecular weight in DOP ($M_w = 35000$, $c = 14\%$, named solution 3) in which we are sure that the chains are overlapped but are too short to create entanglements.

Figure 14a−c represents SANS patterns observed at $D = 10$ m for a series of shear rates at $T = 4$ °C. They definitely show that butterflies are also present for nonentangled semidilute solutions. We observe the same dependence for the onset of the scattering anisotropy with shear rate and temperature as described for solution 1: the anisotropic scattering appears at lower $\dot{\gamma}$ as *T* decreases. We cannot calculate the corresponding *Wi* values since we do not observe any shear thinning in rheology. However, contrary to the observations made with solution 1, $d\Sigma_z/d\Omega(q,\dot{\gamma})$ remains unchanged as the shear rate increases. This can be due to the fact that the chains are not entangled, but it would be necessary to perform other experiments, involving lower temperatures or higher shear rates to confirm this observation. In summary, entanglements at rest are not mandatory for a butterfly-like structure.

It is also interesting to note that, with solution 3, the butterfly effect appears at higher *q* than with solution 1. This could be linked to the dependence of the correlation length at rest with concentration ($\xi_1 \approx c^{-3/4}$). The scattering of a solution at rest is shifted toward larger *q* for high concentrations.

Finally, no irreversibility was observed when the shear was stopped.

4.4.2. More Dilute Solution. As an approach of the dilute regime, we present here SANS measurements on a solution with the same polymer as solution 1, but at lower concentration ($M_w = 572\,000$, $c = 3.5\%$, named solution 2), at the boundary between the dilute and the semidilute regime.

Anisotropic SANS patterns have also been obtained with this solution. We find qualitatively the same behavior as with solution 1. A study at constant temperature ($T = 11$ °C) and increasing shear rates (Figure 15) shows the evolution of the patterns from a butterfly shape to an elliptical shape for shear rates between 250 and 3100 s^{-1}. The corresponding Weissenberg numbers are approximately $Wi = 40$ and 100. These *Wi* are higher than the ones used with solution 1. We did not investigate the different shear effects with this solution as systematically as with solution 1. Nevertheless, we can deduce from our results that higher *Wi* are necessary to obtain an effect with solution 2 as compared to solution 1.

In addition, as a new but still unexplained result for semidilute solutions, we found that high shear rates leading to elliptical patterns induce irreversible structural changes in the solution, at least on the time scale of a day. This feature can be related to the high *Wi* values used. The fact that with solution 2 we can reach such high *Wi* might be explained by the lower first normal stress difference for the same *Wi* compared to

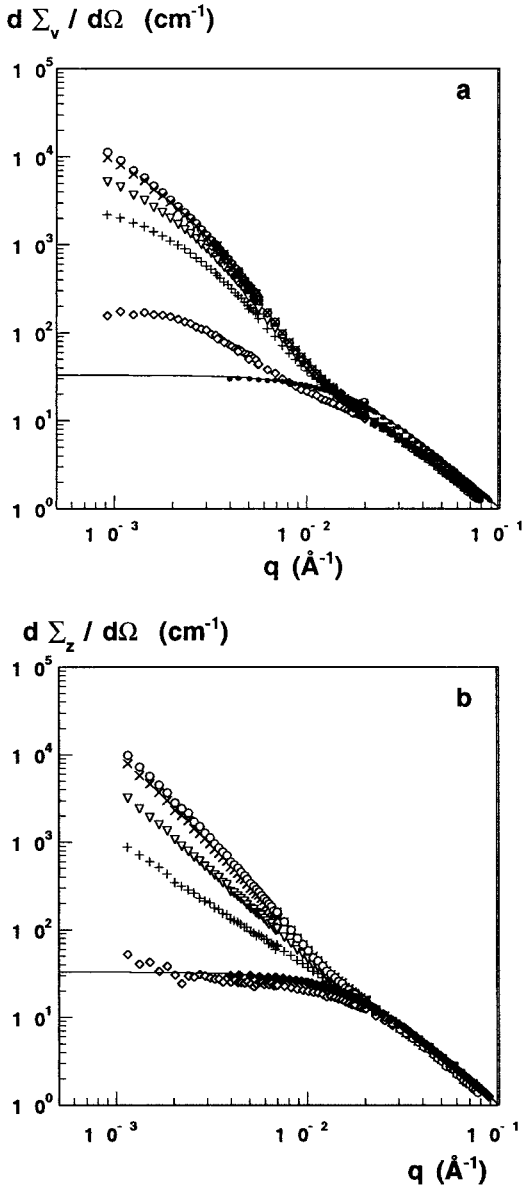

Figure 10. Coherent differential scattering cross section dΣ/dΩ (cm^{-1}) as a function of the momentum transfer q, at $\dot{\gamma} = 165\ s^{-1}$ and several temperatures: $T = 14.7$ °C (○), $T = 15.5$ °C (×), $T = 16.4$ °C (▽), $T = 17.5$ °C (+), and $T = 25.4$ °C (◇), in the v direction (a) and in the z direction (b). The full line is the Ornstein−Zernike fit of $d\Sigma(\dot{\gamma} = 0)/d\Omega$ for $T = 22$ °C.

solution 1. Another explanation for this irreversibility might be that demixing is easier at lower concentration. It is interesting to note that flow-induced permanent demixing has been already observed for a highly dilute polymer solution, though in this experiment no butterfly-like anisotropy was observed.[32]

4.5. Summary. From this whole set of experiments, we can deduce that a combination of temperature and shear rate induces an anisotropic enhancement of scattering. The resulting isointensity contours have the shape of a butterfly. A decrease of the temperature is qualitatively equivalent to an increase of the shear rate; both shift the scattering toward lower q; a further increase of the scattering is observed as the temperature approaches the phase separation at rest for a given Wi. Such changes cannot be related to the parameter Wi only, as seems to be the case for the mechanical functions.

Two effects might increase the scattering in the (v, z) plane: (1) enhanced concentration fluctuations in the direction of flow would lead to a large scattering in the v direction (this is what we observe for the lower shear rates investigated) and (2) demixing, conversely, would lead to a large scattering in all directions. We do not have access to the ∇v direction by SANS, but the large scattering that we observe in the z (or neutral) direction could result from a demixing process.

5. Discussion

Most of the discussion will be devoted to the type of objects and the temperature dependence of the shear-induced effects observed by SANS with solution 1.

5.1. From Scattering to Direct Space: Which Objects? 5.1.1. The High *q* Range. We discuss very briefly the high q range, which we define as corresponding at rest to the inside of the chain. Its observation is indeed possible only at scales at which the chains are not interpenetrated, i.e., at $q > 1/\xi_1$. Under shear, $d\Sigma_v/d\Omega(q,\dot{\gamma})$ decreases, while $d\Sigma_z/d\Omega(q,\dot{\gamma})$ remains equal to the signal at rest. A simple explanation is that under shear we still see the inside of the chain and, therefore, a similar deformation to the ones already observed in polymer melts[31] and dilute solutions:[32] the v direction is the projection of an axis of elongation (at least viewed in our (v, z) plane) for the chain, meanwhile the z direction is neutral.

Similar anisotropy could arise from "objects" seen as regions with a different polymer concentration compared to the surrounding medium. Those could be individually deformed by shear in the range $1/\xi_2 < q < 1/\xi_1$. At $q > 1/\xi_1$, it would mean, however, that the chains are more interpenetrated than at rest, a result which we do not expect from shear deformation.

5.1.2. The Low *q* Range. On the length scale corresponding to low q, shear leads to structural changes in the solution which may be described as some new scattering objects. From the different data (variation of temperature and shear rate), we can distinguish three cases.

(i) At the first stage of the shear effect (at low shear rate and ambient temperature), the variation of the intensity with q in the z direction remains weak (flat asymptote toward $q \rightarrow 0$). Meanwhile, in the v direction, the scattering already increases softly when $q \rightarrow 0$ in such a way that no correlation length can be deduced.

Contours. The intensity levels found along v do not exist along z; therefore, the isointensity curves degenerate in $q = 0$ within a large "dark sector" around the z direction. We will call this result a large indentation, or a narrow waist. On the contrary, the variation with q is limited to a sector along v; therefore, the lobes are very elongated.

Picture of the System. At this stage, one can imagine that the solution is a homogeneous medium, i.e., made of a single liquid phase, with larger spatial concentration fluctuations along the flow. More exactly, the projection of the concentration fluctuations on the (v, z) plane is larger in the v direction. One has a first class of objects with an elongation of the chains in the flow direction, leading to an enhancement of concentration fluctuations in this direction. To the first degree of analysis, this effect can be well described by two different models: (1) the very qualitative picture of greater spatial separation of less deformable zones along v,[31] extended to the case of viscous flow, and (2) the more

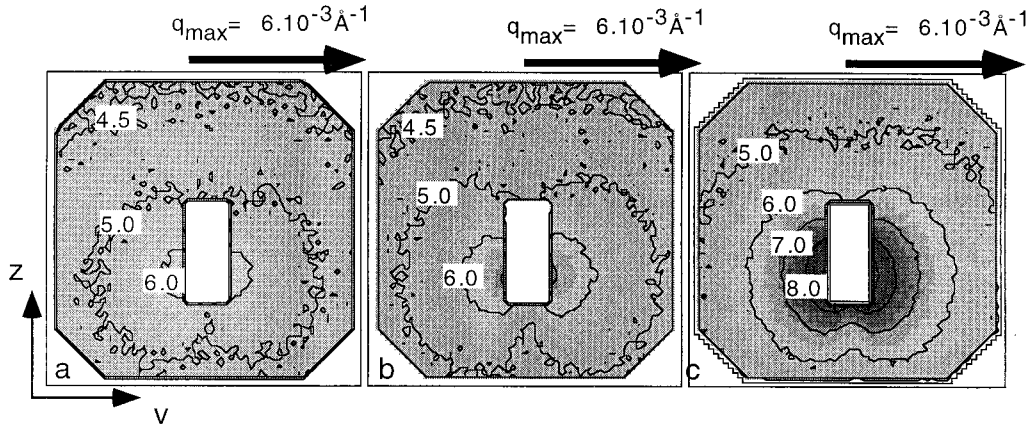

Figure 11. Contour plots of the two-dimensional scattering patterns obtained at $D = 35.7$ m ($\lambda = 10$ Å), at $T = 3.5$ °C and several shear rates $\dot{\gamma} = 0.27-1$ s^{-1} (a), $\dot{\gamma} = 0.89-1$ s^{-1} (b), $\dot{\gamma} = 2.95$ s^{-1} (c).The indicated values are log(dΣ/dΩ).

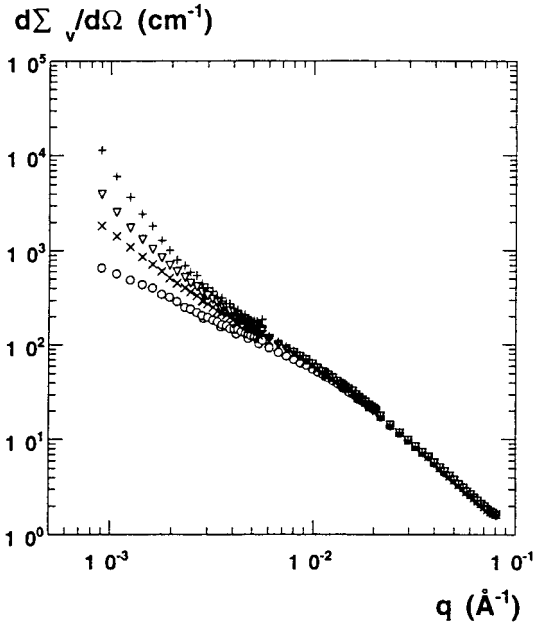

Figure 12. Coherent differential scattering cross section $d\Sigma_v/d\Omega$ (cm^{-1}) as a function of the momentum transfer q, at $\dot{\gamma} = 0.25$ s^{-1} and several temperatures: $T = 3.4$ °C (○), $T = 2.3$ °C (×), $T = 2.0$ °C (▽) and $T = 1.7$ °C (+).

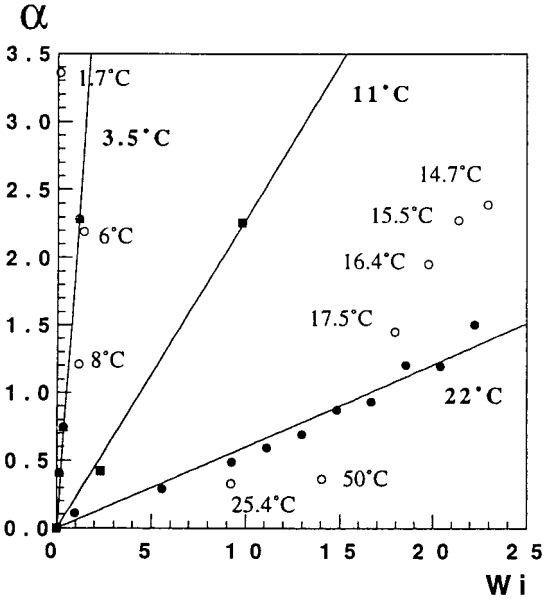

Figure 13. Exponent α as a function of *Wi* for a large range of temperatures between $T = 2$ and $T = 50$ °C.

rigorous approach of Helfand and Fredrickson,[5] which includes a complete mathematical derivation.

Effectively, both approaches predict no change in the *z* direction, since no deformation is applied in this direction.

According to these models, due to an increase of the fluctuations at rest and at temperatures close to phase separation, the system should then be more sensitive to shear. The calculated expression of the Helfand−Fredrickson model actually predicts a divergence of the scattering, which is close to what we observe at lower temperature.

(ii) A second stage of the shear effect is seen for large shear rates around room temperature as well as for low shear rates at low temperature.

At large q in the v direction, it seems that we find a similar elongation as observed at the first stage of the shear effect (i). At lower q, however, in the v direction the scattering is significantly enhanced, which could be interpreted as much larger fluctuations, with a new apparent correlation length Ξ_{Deb} of a few hundred angstroms. The best fit of $d\Sigma_v/d\Omega(q,\dot{\gamma})$ is obtained with the addition of two functions (cf eq 1 and 5): a Lorentzian function and a Debye−Bueche function.

The correlation lengths, denoted ξ_2 and deduced from the Lorentzian fits, are on the same order of magnitude as ξ_1 obtained for the solution at rest, with a slight increase of ξ_2 as the shear rate increases. Let us note that a Lorentzian function is flat at low q.

A Debye−Bueche Function describes the strong increase of the intensity at low q and the following plateau at very low q. The shape of this second function, in the low q range, together with the progressive increase of the slope α in the z direction, suggests that some more compact objects are created under shear. However, so far we do not have any indication about the size of these objects in the z direction.

Contours. Corresponding to the behavior of the radially averaged scattering along a given direction, the shape of the contours changes progressively at this stage of the shear effect: it becomes less elongated along v (the intensity varies faster with q compared to the first stage of the effect (i)) and the indentation is less marked (wider waist) along the z direction because $d\Sigma_z/d\Omega$ now varies with q in contrast to the first stage (i).

Picture of the System. Both the possibility of decomposition of the scattering along v in two contribu-

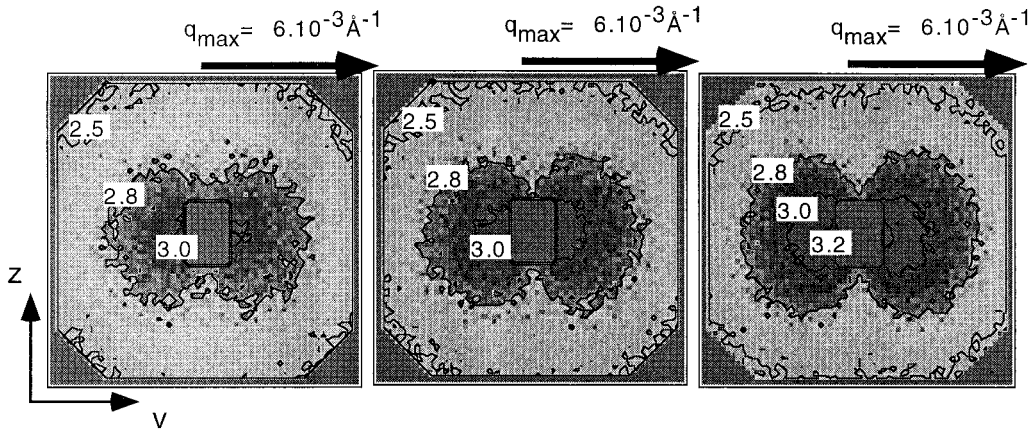

Figure 14. Contour plots of the two-dimensional scattering patterns obtained at $D = 10$ m ($\lambda = 10$ Å), with solution 3 ($M_w = 35\,000$, $c = 14\%$), at $T = 4$ °C and at several shear rates $\dot{\gamma} = 250$ s^{-1} (a), $\dot{\gamma} = 500$ s^{-1} (b), $\dot{\gamma} = 1460$ s^{-1} (c).

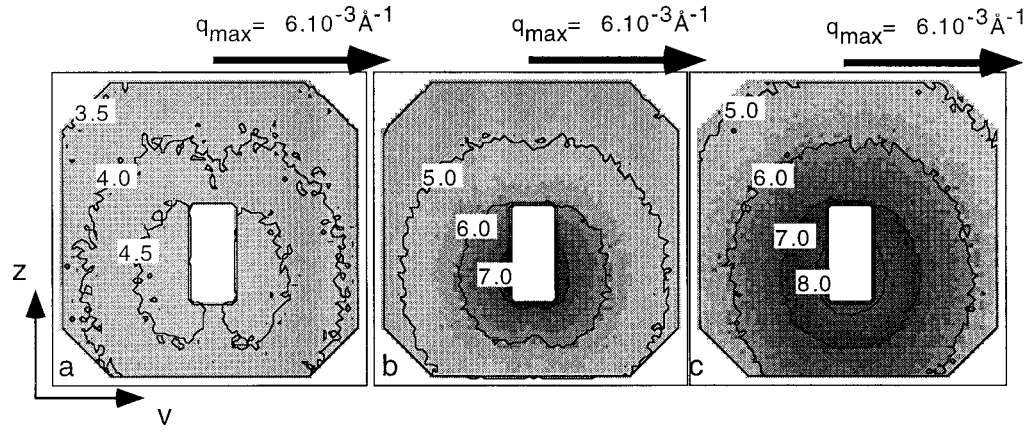

Figure 15. Contour plots of the two-dimensional scattering patterns obtained at $D = 35.7$ m ($\lambda = 10$ Å), with solution 2 ($M_w = 572\,000$, $c = 3.45\%$), at $T = 11$ °C and several shear rates $\dot{\gamma} = 250$ s^{-1} (a), $\dot{\gamma} = 500$ s^{-1} (b), $\dot{\gamma} = 1645$ s^{-1} (c).

tions and the increase in scattering along z disagree with the picture of a simple spatial separation as well as with the HF model. We have left their domain of validity, and other processes occur.

(iii) The third stage of the shear effect is visible mostly at low temperature.

The increase of the intensity is now very strong in both directions, z and v.

In the z direction, the slope α becomes as high as 3.4. Let us recall that Porod's law is in q^{-4}. Values lower than 4 are often attributed to slightly fractal-like surfaces or to polydispersity effects. However, values of 3.4 or close to 4 suggest also that the objects are very compact in the z direction.

The signal in the v direction is comparable to the one along z but with no definite slope in the explored q range.

Contours. Under these conditions, the contours display a third type of shape. In most of the detector area, they are slightly elliptic with the larger axis along the z direction. Only a very faint indentation remains at the lowest q values. Thus, if present, the butterfly type correlations are centered at lower q. From this shape, one can conclude a grain coarsening of the structure. In some cases (Figure 9c), the envelopes of the butterflies (at larger q) have a pronounced elliptical shape: this can be due to the fact that the individual objects are elongated along v or that short scale inter-object correlations undergo elongation along v.

Picture of the System. Since no correlation length can be extracted from the data in both directions in the range of q available by SANS, we can suppose that the compact objects created are larger than 500 Å. As we will see in section 5.2.1, at this stage of the shear effect, these objects are not visible by SALS and therefore do not exceed the size of about 1 μm.

Nevertheless, even if the scattering is dominated by objects having a particular size, it is possible that other scatterers are present in solution. There could be a coexistence of objects of different sizes, or even of compact objects together with concentration fluctuations. This would explain why the intensity at intermediate and large q under shear and in both directions v and z (apart to the anisotropy due to chain elongation) never decreases significantly in our SANS measurements compared to the signal at rest. Indeed, if the objects were growing in size at constant volume fraction, their contribution to the cross section would increase at small q (below the accessible values) and decrease at larger q: their scattering would eventually vanish in the accessible q window.

The butterfly patterns seem now to be due to anisotropic correlations between large objects, which may be some droplets with higher polymer concentration. Though the type of diffusing objects seems different for low shear (fluctuations, Figure 9a) and for large shear (droplets, Figure 9b), similar anisotropic patterns are observed due to stronger correlations along the v than along the z direction in both cases. Depending on the experimental conditions, such a butterfly shape is observed in our study in different q windows.

5.1.3. Volume Fractions and Contrast. A good characterization of the objects present in the solution would imply the knowledge of their size, their number, and their composition. We have remarked above that, if the size R of compact objects grows at constant volume fraction, the Porod or Debye−Bueche law predicts a signal proportional to the specific area which decreases at $q > 1/R$. Compared to the intensity at rest, we do not observe any decrease in the intermediate q range. It is indeed possible that objects, when seen as regions of higher concentration, become more numerous. There can also exist a distribution in sizes between the big objects and some new smaller ones, simultaneously formed under shear.

The composition may also depend on the flow conditions. Knowing that scattering objects are regions rich or poor in deuterated polymer, we can estimate some combination of the contrast and the volume fraction, for the simple case of a random diphasic system. SANS allows us to obtain the scattering cross section in absolute units. It can then be written as follows[33]

$$d\Sigma_{DB}/d\Omega(q) = 8\pi\Xi^3 K_{eff}^2 \phi(1-\phi)/(1+(q\Xi)^2)^2 \quad (6)$$

where ϕ is the volume fraction of one phase, Ξ is the correlation length, and K_{eff}^2 is the contrast between the two phases, of polymer volume fraction ϕ_{rich} and ϕ_{poor},

$$K_{eff}^2 = K_{max}^2(\phi_{rich} - \phi_{poor})^2 \quad (7)$$

K_{max}^2, the contrast between pure polymer and pure solvent, is known. For any case where we can determine both $d\Sigma_{DB}/d\Omega(q=0)$ and Ξ, we can obtain the product:

$$K_{eff}^2 \phi(1-\phi)/K_{max}^2 = (\phi_{rich} - \phi_{poor})^2 \phi(1-\phi) \quad (8)$$

The right-hand side of the latter equation is equal to $-(\delta\phi_{rich}\delta\phi_{poor})$ from the conditions of conservation of polymer mass.

We can take as an example from the third line of Table 2, $d\Sigma_{DB}/d\Omega(q=0) = 3206\ cm^{-1}$, and $\Xi = 343$ Å. We find $K_{eff}^2\phi(1-\phi) = 3 \times 10^{18}\ cm^{-4}$. As $K_{max}^2 = 32.4 \times 10^{20}\ cm^{-4}$, the quantity $(\delta\phi_{rich}\delta\phi_{poor})$ is close to 10^{-3}. In a symmetric case, this would give $(\delta\phi_{rich} = \delta\phi_{poor})$ around 3%, i.e., two phases of $(9-3) = 6\%$ and of $(9+3) = 12\%$, therefore being in the semidilute regime. On the contrary, if we adopt the hypothesis that the decomposition in two phases follows the coexistence curve obtained at rest (Figure 2; note that this assumes a shift of the cloud point independent of the concentration, which was not observed by Verstrate and Philippoff), we can assume that the poor phase will be around a few percent, e.g. 2% (in the dilute regime). The enrichment of the rich phase, $\delta\phi_{rich}$, will then be around 1.4% ($\phi_{rich} \approx 10.4\%$), which is a realistic value. In this case, the volume fraction of the polymer rich phase is around 84%. This would mean that the continuous phase is the rich one, with "pores" of lower concentration inside.

Such estimates can only be done if the fit of the low q regime with a Debye−Bueche function is possible, as for the results given in Table 2. For larger shear, neither Ξ nor the zero q limit of $d\Sigma/d\Omega(q)$ can be determined as we observe an increase for both; it seems, however, that the ratio $d\Sigma_{DB}/d\Omega(q=0)/\Xi^3$, and therefore the effective contrast, may not change by a huge factor.

5.1.4. Time−Temperature Superposition. After renormalization of the shear rate by the terminal time at each temperature, using the parameter Wi, we see that the scattering is more and more sensitive to shear when the temperature is lowered (cf. section 4.3). Knowing $T_\Theta \approx 7$ °C and $T_{cloud} \approx -6$ °C, it seems that this increased sensitivity is driven by the approach of the coexistence line (note that the difference between Θ and T_{cloud} is still large for our molecular weight (572 000), but it could be smaller for larger molecular weights). As the coexistence line is approached, for the same shear rate, larger and more compact objects are created.

We can assume two different origins for the large objects: (i) either enhancement of the concentration fluctuations diverge finally and transform into a phase separation (ii) or, as in the theory of Verstrate and Philippoff, the deformation of the chains induces a change in the free energy of mixing which itself induces a phase separation at $T > T_{cloud}$. Let us note that, if phase separation is triggered separately, the structure of the solution should in turn be deformed by shear. This deformation could lead to butterflies.

Option i is the simplest, since it involves only one process, which can perfectly diverge (this is predicted by simple mean field theory, as in the HF model). Option ii is possible; it should in principle produce an abrupt change at a given temperature. This is not observed. If we examine a set of data at constant Wi, we see no abrupt transition for decreasing temperatures.

5.2. Connection with Light Techniques. As forecast above, comparison with experiments using light (see section 1) is difficult, because of the many differences coming from the solution itself (T_Θ point, temperatures, molecular weights, and concentrations, leading to unknown values of τ_r and Wi) and from the geometry of the experimental setups (detection plane, q range).

5.2.1. Comparison with SALS. First of all, the more marked similarity is the shape of the butterfly patterns in the (v, z) plane as obtained with SANS as well as SALS. For SALS, the interpretation of such anisotropy, in terms of either concentrated zones inside region of less concentrated or droplets being preferentially correlated along the vorticity direction at low shear rates, is close to the one given for SANS.

A precise comparison between SANS and SALS techniques is possible with the preliminary SALS measurements which we performed on solution 1 in collaboration with the group of Richtering (U. Freiburg, Germany), using a cone and plate cell (a description of this apparatus can be found in ref 34).

Our first observation is that no changes with respect to the scattering at rest are visible by SALS, even in the range of $(\dot\gamma, T)$ conditions where we observed the strongest SANS effects (indicating that SANS has a good sensitivity on a length scale below the one of SALS). Since high shear rates could not be obtained with this rheometer, the temperature had to be lowered into a range close to T_{cloud} in order to observe butterfly patterns, e.g. $T \approx -5$ °C, for $\dot\gamma = 30\ s^{-1}$, $Wi \approx 27$, or $T \approx -7$ °C, for $\dot\gamma = 10\ s^{-1}$, $Wi \approx 11$. Though the solution was always clear at rest, a strong turbidity became visible under shear. Such severe conditions could not be attained with the SANS Couette cell, which is restricted due to Weissenberg instabilities. In summary, for solution 1, common $(T, \dot\gamma)$ conditions where

an anisotropic signal could be observed by both SANS and SALS could not be reached. These observations confirm that a coarsening of the structure as observed by SANS may be necessary to make it visible by SALS. However it seems to us, but has yet to be established, that neutron scattering would also remain strong for the conditions where shear effects are observed by SALS.

Comparisons can also be made with the literature. Hashimoto et al.[14] see SALS butterflies at ambient temperature, with nondeuterated PS, smaller concentration, but larger molecular weights. Several values of molecular weight were used, ranging from around 3×10^6, up to around 10^7 (these solutions separate soon below Θ, since the width of the Θ regime varies as $1/M_w$). Let us discuss here the data of ref 14, measured at $T = 22$ °C for molecular weights close to 5.5×10^6 and 3.5×10^6 and two concentrations. The phenomena are stronger and more clear-cut for large M_w and large concentration. The onset of an increase the integrated intensity in the v direction at $\dot{\gamma}_c$ coincides always with the onset of shear thinning, i.e., $\dot{\gamma}_c$ corresponds to $Wi = 1$, at which changes in SANS are noticeable. For $Wi > 1$, the scattered light increases progressively with shear rate, as the SANS intensity does.

However, butterflies become well detectable (depending upon the device) at much larger Wi (10−50), close to the shear rate noted, $\dot{\gamma}_a$. Many processes, such as the onset of a second increase of integrated intensities along both the v and z directions or the onset of the shear-induced cloudiness, occur around this particular shear rate. This regime is not far from the growth of a light streak along z, due to the formation of strings along v (which coincides with an increase of the viscosity). The scattered light is then very large in most directions and might correspond to the observation of Verstrate and Philippoff[2] (which was anyhow not sensitive to the anisotropy of the scattering). The values of Wi for $\dot{\gamma}_a$ (100 or more for $M_w > 10^6$, at $T = 22$ °C) are larger than the largest Wi we investigated in our SANS measurements (25 at this temperature). This is not surprising because the relation between SANS and SALS is governed by the different sizes of the most detectable objects visible by these two techniques.

The striking fact here is that scattering with similar butterfly shape is detected over such a large q range. In practice it depends on the shear regime. In the first regime of low shear, where an increase of integrated intensity is detected by SANS, a rather small SALS could correspond to what SANS is displaying strongly. On the other hand, it is not obvious that the structure responsible for large SALS could still give large SANS, unless small objects coexist with larger ones. This concerns only the largest shears observed by SANS, close to the upper part of the ($\dot{\gamma}_c$, $\dot{\gamma}_a$) range defined by Hashimoto et al.,[16−18] where SALS butterflies are strongly visible. Anyhow, for shear rates closer to $\dot{\gamma}_a$ and above, we have no SANS data.

Microscopy seems to detect the structure responsible for the butterflies as soon as the latter can be detected via SALS.[18] It shows rather compact objects, but this may be due to image treatment. Above $\dot{\gamma}_a$, the string regime is the same as for phase-separated systems under shear; one can infer that the solution is phase-separated in droplets of micron size. However, our SANS measurements tend to show that phase separation occurs at a lower shear rate than $\dot{\gamma}_a$.

5.2.2. Comparison with WALS. Comparison with WALS can be done using refs 6, 20, and 21. It seems that WALS observations are made in similar regimes as the neutron ones and show phenomena of comparable importance. A reason might be that the two q ranges are quite close.

The WALS work is done with a polymer of $M_w = 1.8 \times 10^6$ and a concentration of 4%[6,20] at $T = 15$ °C (only 5 °C above the cloud point, $T_{cloud} = 10$ °C). This gives a relaxation time $\tau_r = 0.57$ s. Shear-induced scattering is seen as soon as $\dot{\gamma} \geq 0.2$ s^{-1} ($Wi \geq 0.12$) in a low shear regime; a new "moderate shear" regime appears above $\dot{\gamma}_{WALS1} \geq 4$ s^{-1} ($Wi \geq 2.35$), where the normal stress becomes larger than the shear stress. There is a definite increase of the scattering at all q, with a rotation of the peaks from the first and third quadrant to the fourth and second one in the (v, ∇v) plane.

Further experiments[21] investigated a transition between the moderate shear regime (above $\dot{\gamma}_{WALS1} = 25$ s^{-1} for the lower molecular weight used in ref 21, $M_w = 1.03 \times 10^6$, giving $\tau_r \approx 0.09$ s^{-1}) and a high shear regime, above $\dot{\gamma}_{WALS2} = 70$ s^{-1}. In this third regime, steady flow and transient flow measurements show that the scattering can be decomposed in two contributions: one has the same level of intensity and the same symmetry as observed in the "moderate shear" range. The second gives a much stronger intensity, a different pattern (four peaks in the four quadrants of the (v, ∇v) plane), and shows a slow coarsening with time. This coarsening proceeds in such a way that the four peaks merge into two peaks along the v axis. Pine et al.[21] conclude that two effects are responsible for the scattering in this regime of shear: one being due to the concentration fluctuations of the intermediate shear range, the other one, appearing at larger shear rates, being due to demixing. Similar possible situations were evoked above. We do, however, not believe to have really explored by SANS a temperature close enough to T_{cloud} (15 °C = $T_{cloud} + 5$ °C in refs 6, 20, 21, $T = T_{cloud} + 5$ °C = −1 °C, where we do not have experimental results); the Weissenberg number for $\dot{\gamma}_{WALS2} = 70$ s^{-1} is $Wi > 7$, a value which we did not reach in this temperature range. This regime may correspond to a fourth stage of the shear effect, following what we called above stage iii.

5.3. Comparison with Mechanical Behavior. Another striking feature is the fact that mechanical properties under steady shear flow follow a time−temperature superposition. On the contrary to scattering, they depend only on the Weissenberg number. It thus seems that the concentration fluctuations are not large enough to modify the mechanical response. This may be due to an insufficient variation of the polymer concentration between polymer rich and polymer poor phases. This would indicate that the estimations of section 5.1.3 assuming a symmetric separation in two phases are more probable than the one assuming that the poor phase is in the dilute regime. Let us note, however, that $|\eta^*|$ is not very sensitive to heterogeneity in composition. Only $G'(\omega)$ indicates the presence of a demixing in polymer solutions, at frequencies where its contribution to $|\eta^*|$ is weak compared to $G''(\omega)$.[35,36]

5.4. Other Solutions. Solutions 2 and 3, which we investigated, show additional interesting features. We see that the different stages of the shear effect as defined for solution 1, are also present at lower concentration (solution 2). However, from the comparison of the experiments made at $T = 11$ °C with solutions 1

and 2, it appears that the Weissenberg number is larger with solution 2 for a similar scattering pattern (for instance, the butterfly shape is still visible with solution 2 for $Wi = 40$). The highest value of Wi that we were able to obtain with solution 2 is 100, yielding elliptical isointensity curves and leading eventually to an irreversible demixing process. This new feature can evidently be due to the high value of Wi. The result would suggest that we could probably observe such permanent changes with solution 1 if the Weissenberg instabilities did not impede reaching high shear rates.

Let us note, however, that no irreversibility was mentioned in any of the SALS[14−18] and SANS[26,27] experiments which deal with strong shear effects for semidilute solutions, although this feature was observed under shear by SANS for a dilute solution.[32] It seems, therefore, that the irreversibility is rather a consequence of the approach of the dilute regime. We try again to quantify the concentration fluctuations involved in this process in order to understand what could lead to this difference. We fit $d\Sigma_v/d\Omega$ with the sum of a Lorentzian function and a Debye−Bueche function. The values obtained for $T = 11$ °C and $\dot{\gamma} = 100$ s^{-1} are $\Xi_{deb} = 460$ Å and $d\Sigma_{DB}/d\Omega(0) = 2730$ cm^{-1}. From the equations of section 5.1.3, we obtain in the symmetric case, $\phi_{rich} = 5.15\%$ and $\phi_{poor} = 1.75\%$, corresponding respectively to the semidilute and the dilute regime. The largest difference between this result and the one obtained with solution 1 is the value of the volume fraction of each phase, under the condition that the poor region would be in the dilute regime. The volume fraction of the rich phase can be as low as $\phi = 0.5$ for solution 2; it is $\phi = 0.84$ for solution 1 if we fix $\phi_{poor} = 2\%$. The topology of these two solutions is certainly very different: in solution 1, one chain could be located in several rich regions. On the contrary, in solution 2 the rich regions are spatially more separated.

With the nonentangled solution 3 (smaller molecular weight), we do not observe all of the different stages of the shear effect. Only the first stage, corresponding to an increase of the intensity in the v direction is obtained. This feature, which agrees with the Helfand−Fredrickson model, had never been observed experimentally with a low molecular weight polymer. It is a clear indication that entanglements are not mandatory to obtain shear-induced structures. From our experiments, we could not conclude that this anisotropy would lead to a stronger scattering as for the entangled solutions, since experiments close to T_{cloud} were not possible with this sample.

6. Summary and Conclusion

Our SANS work reveals that generation of a flow-induced anisotropic structure at a length scale between 10 and 500 Å is quite general behavior for semidilute solutions. It is observable (1) from 40 °C above the Θ temperature down to 5 °C below it (i.e., in a large range of temperatures, probably above the Θ regime, i.e., good solvent, as much as below, very close to the coexistence line), (2) in the semidilute concentration range up to the boundary with the dilute region, and (3) with and without entanglements.

However, each situation has its specificity from the experimental point of view: (1) for unentangled solutions, only one regime, with a simple increase of concentration fluctuations could be clearly observed, (2) for entangled solutions, a second regime, even a third, where the induced structures coarsen as the shear rate increases, are explored, and (3) for solutions close to the dilute regime, conditions similar to the second or third regime seem to produce some specific irreversibility.

Though the comparison between these different situations is interesting and was not done before by other techniques, the main part of the paper is dedicated to the first system, fully in the entangled and semidilute regime. The central question is the origin of the effect; i.e., is it simply rheology, which would modify the concentration fluctuations, or thermodynamics, if the chain deformation was modifying the free energy of mixing?

Aiming to give an answer to this question, we have tried to check the effect of temperature by piling up enough observations as a function of $\dot{\gamma}$ and T. If the origin of the shear-induced anisotropic structure is rheology, the temperature should just modify the characteristic times, that is to say we should observe a time−temperature superposition. In practice, approaching the demixing temperature at rest remains a strong promoter of shear effects after time−temperature correction.

Another task is to link our SANS observations to those obtained from light scattering, done under different conditions. From comparison with other groups' results and our SALS experiments, it is clear that flow affects first the concentration fluctuations at low length scale. SANS is therefore very sensitive for the study of "initial stages".

WALS shows effects quite similar to the ones observed by SANS (in a different v, ∇v plane) and distinguishes three stages.

Small angle light scattering (SALS) appears faintly at low shear rates and is very strong at highest shear rates. It is likely that the structural reorganization tends toward a diphasic system, which could be a coarsening of the structure observed at earlier stages by SANS. This is also suggested by light microscopy. It is also interesting to note that the increasing anisotropic light scattering leads to a turbidity of the solution, directly visible by the eye. The effect appears in a surprisingly large range of temperature and shear rates, involving a large range of sizes. Similar butterfly patterns, though not due to the same objects, can be observed under various experimental conditions. SANS and SALS observations under exactly the same conditions should be done in order to confirm the impression that objects of different sizes could coexist under shear.

Though the approach of coexistence curve at rest makes the system very sensitive to shear, the origin of demixing is still not established. At this point it seems to us that a divergence of a Helfand−Fredrickson-type effect is better supported by facts than a purely thermodynamic origin (free energy of mixing of one chain). Among further information to look for, the conformation of a single chain under shear is the next step which we plan to investigate.

References and Notes

(1) Daoud, M.; Jannink, G. *J. Phys. Fr.* **1976**, *37*, 973−979.
(2) Verstrate, G.; Philippoff, W. *J. Pol. Sci., Pol. Lett. Ed.* **1974**, *12*, 267−275.
(3) Rangel-Nafaile, C.; Metzner, A.; Wissbrun, K. *Macromolecules* **1984**, *17*, 1187−1195.
(4) Rofe, C.; Lambert, R.; Callaghan, P. *J. Rheol.* **1994**, *38*, 875−887.
(5) Helfand, E.; Fredrickson, G. *Phys. Rev. Lett.* **1989**, *62*, 2468−2471.

(6) Wu, X.; Pine, D.; Dixon, P. *Phys. Rev. Lett.* **1991**, *66*, 2408−2411.
(7) Van Egmond; Werner, D.; Fuller, G. *J. Chem. Phys.* **1992**, *96*, 7742−7757.
(8) Milner, S. *Phys. Rev. Lett.* **1991**, *66*, 1477−1480.
(9) Brochard, F.; de Gennes, P. G. *Physicochem. Hydrodyn.* **1983**, *4*, 313−322.
(10) Doi, M.; Onuki, M. *J. Phys. II, Fr. 2* **1992**, 1631−1656.
(11) Ji, H.; Helfand, E. *Macromolecules* **1995**, *28*, 3869−3880.
(12) Van Egmond, J. *Macromolecules* **1997**, *30*, 8045−8057.
(13) Onuki, M. *J. Phys. Cond. Matter* **1997**, *9*, 6119−6157.
(14) Kume, T.; Hashimoto, T.; Takahashi, T.; Fuller, G. *Macromolecules* **1997**, *32*, 77232-7236.
(15) Hashimoto, T.; Fujioka, K. *J. Phys. Soc. Jpn.* **1991**, *60*, 356−359.
(16) Hashimoto, T.; Kume, T. *J. Phys. Soc. Jpn.* **1992**, *61*, 1839−1843.
(17) Kume, T.; Hashimoto, T. In *Flow induced Structure in polymers*; Nakatani, A., Dadmun, M., Eds.; ACS: Washington, DC, 1995; Chapter 3.
(18) Moses, E.; Kume, T.; Hashimoto, T. *Phys. Rev. Lett.* **1994**, *72*, 2037−2040.
(19) Han, C. Critical polymer mixtures under flow. SASFLOW'98, ESRF−ILL workshop, May 98, Grenoble, France.
(20) Dixon, P.; Pine, D.; Wu, X. *Phys. Rev. Lett* **1992**, *68*, 14, 2239−2242.
(21) Migler, K.; Liu, C.; Pine, D. *Macromolecules* **1996**, *29*, 1422−1432.
(22) Yanase, H.; Moldenaers, P.; Mewis, J.; Abetz, V.; Van Egmond, J.; Fuller, G. *Rheol. Acta* **1991**, *30*, 89−97.
(23) Moldenaers, P.; Yanase, H.; Mewis, J.; Fuller, G.; Lee, C.; Magda, J. *Rheol. Acta* **1993**, *32*, 1−8.
(24) Hammouda, B.; Nakatani, A.; Waldow, D.; Han, C. *Macromolecules* **1992**, *25*, 2903−2906.
(25) Nakatani, A.; Douglas, J.; Ban, Y.; Han, C. *J. Chem. Phys.* **1994**, *100*, 3224−3232.
(26) Boué, F.; Lindner, P. *Europhys. Lett.* **1994**, *25*, 412−427.
(27) Boué, F.; Lindner, P. In *Flow induced Structure in polymers*; Nakatani, A., Dadmun, M., Eds.; ACS: Washington, DC, 1995; Chapter 4.
(28) Park, J. O.; Berry, G. C. *Macromolecules* **1989**, *22*, 3022−3029.
(29) Baumgartel, M.; Willenbacher, N.; *Rheol. Acta* **1996**, *35*, 168−185.
(30) Lindner, P.; Oberthür, R. *Colloid Polym. Sci.* **1985**, *263*, 443−453.
(31) Mendes, E.; Lindner, P.; Buzier, M.; Boué, F.; Bastide, J. *Phys. Rev. Lett.* **1991**, *66*, 1595−1598.
(32) Lindner, P. *Physica A* **1991**, *174*, 74−93.
(33) Lal, J.; Widmaier, J. M.; Bastide, J.; Boué, F. *Macromolecules* **1994**, *27*, 6443−6451.
(34) Berghausen, J.; Fuchs, J.; Richtering, W. *Macromolecules* **1997**, *30*, 7574−7581.
(35) Palierne, J. F. *Rheol. Acta* **1990**, *29*, 204−214.
(36) Muller, R. Modèles d'Émulsion Appliqués à la Rhéologie des Mélanges de Polymères. 33eme colloque annuel du groupe francais de rhéologie, Biarritz, Oct. 12−14, 1998.

MA981882D